Generation of phase-controlled ultraviolet pulses and characterization by a simple autocorrelator setup

Moehring, J.; Buckup, T.; Lehmann, C.S.; Motzkus, M.

published in
Journal of the Optical Society of America. B: Optical Physics
2009

DOI (link to publisher)
10.1364/JOSAB.26.001538

document version
Publisher's PDF, also known as Version of record

Generation of phase-controlled ultraviolet pulses and characterization by a simple autocorrelator setup

Jens Möhring,[1] Tiago Buckup,[1] C. Stefan Lehmann,[1,2] and Marcus Motzkus[1,*]

[1]*Physikalische Chemie, Fachbereich Chemie, Philipps-Universität Marburg, Hans-Meerwein-Strasse, D-35043 Marburg, Germany*

[2]*Present address: Department of Chemistry and Laser Centre, Vrije University, de Boelealaan 1083, 1081 HV Amsterdam, The Netherlands*

[*]*Corresponding author: Marcus.Motzkus@pci.uni-heidelberg.de*

Received April 24, 2009; revised June 2, 2009; accepted June 2, 2009; posted June 5, 2009 (Doc. ID 110580); published July 8, 2009

A versatile femtosecond ultraviolet (UV) pulse generation, a phase modulation, and a characterization setup for coherent control applications are demonstrated. For high-performance phase control of ultrashort pulses direct in the UV a microelectromechanical-system-based 2D mirror array is applied. Multiple examples for successful phase control of ultrashort UV pulses are given, such as arbitrarily phase tailoring and pulse recompression in open and closed loop schemes. For simple and effective characterization of the generated pulses, a UV autocorrelator based on two-photon absorption in a solar blind photomultiplier is constructed. The effects of space–time coupling on split mirror autocorrelation measurements are addressed and minimized. © 2009 Optical Society of America

OCIS codes: 190.4970, 190.7110, 190.7220, 320.5540, 320.5520, 320.7160.

1. INTRODUCTION

Generation of phase-modulated femtosecond ultraviolet (UV) pulses represents a key technology to study a great number of highly relevant molecular systems and photochemical reactions with the methods of coherent control and advanced nonlinear spectroscopy techniques [1,2]. For coherent control experiments in the UV, a wavelength tunable assembly for ultrashort UV pulse generation and an associated characterization must be combined with the appropriate phase modulation technology. These methods must solve the constraints of conventional shaping technologies in the UV and the challenge of low energy characterization in this spectral range. Furthermore, the complete configuration has to be simple and robust enough to provide sufficient measuring time for the actual spectroscopic or control experiment. Therefore, the present paper illustrates a full setup of an UV source, a modulator, and a characterization, capable of satisfying these requirements.

To gain access to modulated femtosecond pulses the output of an ultrashort UV pulse generator, relying on parametric processes, is fed into a direct UV-shaping spatial light modulator (SLM) setup. Owing to the opacity of most phase modulators in the UV spectral range, a special phase modulation technology has to be used here. One possibility to overcome this issue is the application of indirect shaping schemes, where shaping takes place in the visible (VIS) spectral region [3–7]. However, this concept is rather complex and limited by the optical convolution taking place during the nonlinear process, leading to coupling between amplitude and phase or to reduction in spectral resolution of the applied shaping. For direct UV phase modulation, acousto-optic modulators or reflective devices are required, which show enough transmission or reflectivity in the UV spectral region, respectively [8–12]. The first direct UV phase modulation was shown with a microelectromechanical system (MEMS) array, which combines phase wrapping and a comparable high density of actuators enabling complex phase synthesis [8]. Furthermore, fast frame rates beyond the timing of typical LCD devices are available with such micromirror arrays. Here we show an improved setup based on this MEMS phase modulator to generate shaped tunable ultrashort UV pulses and discuss its advantages and limitations.

The precise application of ultrafast UV pulses, especially of shaped pulse forms, requires a reliable characterization technique to verify the experimental conditions on a daily basis and to support setup operations. Especially, the adjustment of the shaper setup or the validation of the generated pulse forms requires a versatile pulse characterization setup. There are various UV pulse characterization devices available relying on external reference pulses [13,14]. Particularly in the context of monitoring a tuning process, which induces optical path length variations, such as the adjustment of typical pulse compressors, characterization with external references is often cumbersome. Autoreferencing capable UV characterization methods, such as frequency resolved optical gating (FROG), are often relying on third-order nonlinearities as phase-matching materials for second-order processes are hardly available in the UV region. Therefore, they demand frequently high intensities or the complex implementation of three-beam setups like in the case of transient grating FROG [15–18]. Autocorrelation devices

represent an easy adjustable characterization setup particularly if a two-photon absorption (TPA) detector is used, since hereby no phase-matching condition has to be set. As TPA based detectors are frequently used for AC measurements in the VIS and the near-infrared (NIR) spectral regions [19–21], it is desirable to extend their usage to the UV spectral range. To enable TPA based nonlinear detectors in the UV, high bandgap materials such as diamond, fused silica (FS), or CsTe have to be used as active media [22,23]. As this group of materials is often applied for the construction of solar blind photomultiplier tube cathodes, the two-photon photoemission in these devices can be exploited as autocorrelation detector. A proof of principle experiment has been recently conducted by Ihara *et al.*, although pulse energies above the damage threshold of the photomultiplier (PMT) were applied to obtain autocorrelation traces [24]. In the present paper we show an autocorrelator setup of a split mirror autocorrelation device based on a solar blind PMT as nonlinear detector. The reduced degrees of freedom compared with other UV characterization devices renders this AC setup well suited to obtain everyday pulse validation and to simplify setup tuning in a coherent control application. Besides the construction of an UV phase modulation and a characterization setup, its features, discussed by shaping examples, are shown in Sections 2 and 3.

2. REALIZATION AND DISCUSSION OF THE EXPERIMENTAL SETUP

Figure 1 shows a complete overview of the presented UV setup. Subsections 2.A–2.C will address the individual components of the setup with special focus on the phase modulator and the pulse characterization technologies applied.

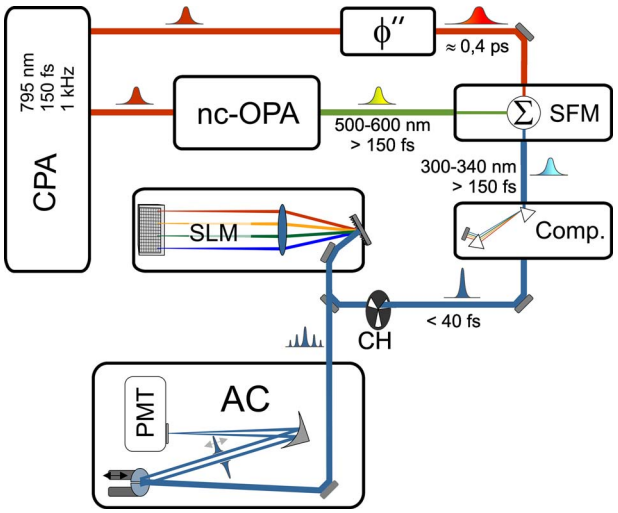

Fig. 1. (Color online) Experimental setup overview. A nc-OPA is pumped by an amplified femtosecond laser (CPA). Tunable VIS radiation is generated and SFM with the temporal stretched (ϕ" indicates a glass block) NIR fundamental without prior pulse compression. Pulse compression is conducted in a UV prism compressor (Comp.). The compressed pulse is fed into our purely reflective 4-f MEMS shaper setup (SLM). A chopper (CH) with a 1:5 duty cycle is used to enable synchronization of the MEMS deflection. The shaped UV pulse is fed to a split mirror TPA (TPA in PMT) autocorrelator.

A. UV Pulse Generation

The initial laser source of the present experiment is a chirped pulse amplifier (Clark MXR 1000), which delivers 130 fs NIR pulses (795 nm/650 μJ). To enable sufficient tunability for spectroscopic and coherent control applications, sum frequency mixing of the output from a noncollinear parametric amplifier was chosen. The UV generation setup consists of a single stage noncollinear optical parametric amplifier (nc-OPA), a sum frequency mixer (SFM), and a UV compressor (Fig. 1). Upconversion by sum frequency mixing uses uncompressed nc-OPA pulses and all pulse compression takes place in the UV [25].

The parametric amplifier generates pulses from below 500 nm to above 600 nm. When mixed with 795 nm NIR fundamental from the CPA system, this corresponds currently to a potential UV tuning range from below 300 nm to above 350 nm. To avoid spectral narrowing effects and to exploit the energy present in the VIS pulse, the NIR beam is chirped to about 0.4 ps before the SFM stage [25]. Based on the SFM in the applied ß-barium borate (BBO) crystal (100 μm, θ=37°), pulse durations below 23 fs can be achieved, purely by UV pulse compression, without the application of the SLM setup.

As the subsequent UV prism compressor needs horizontal input polarization to exploit Brewster conditions in the FS prisms, the polarizations of the VIS and the NIR beams are rotated by 90° with achromatic $\lambda/2$ phase retarders in front of the SFM stage. UV energies of up to 500 nJ are accessible directly after the SFM stage, yielding energies of up to 250 nJ behind the compressor.

B. MEMS Phase Modulator

After the compressor, the pulse is fed into a phase modulator based on a MEMS chip. This phase modulator (Fraunhofer/IPMS, 2D MEMS phase former kit) allows for direct UV pulse shaping down to about 200 nm, limited only by the reflectivity of the aluminum mirror surface [8]. In contrast to nonpixelated devices such as deformable mirrors, the 2D-MEMS microstructured mirror allows phase wrapping, which is necessary to synthesize more complex phase functions in coherent control applications.

Defined by the MEMS modulator operation principle, the shaper setup is built in reflective 4-f geometry, with a cylindrical mirror (f=254 mm, illustrated in Fig. 1 by a lens symbol) and a grating with a groove density of 1200 1/mm. For the illustration of the space–time coupling effects, a similar shaper geometry based on a 600 g/mm grating and a f=500 mm mirror has been used.

Owing to hardware limitations of the MEMS array the modulator permits only a temporal duty cycle of 5%. As the minimum deflection time of the shaper is 0.2 ms, it is possible to synchronize the SLM to the laser to gain an effective pulse usage ratio of 20% on a 1 kHz laser system. All unmodulated pulses are removed by a chopper blade with an appropriate duty cycle. In the current setup, the 2D shaping is not exploited and all pixels in a column are set to equal values.

The deflection calibration was done by a Michelson interferometer setup, relying on a HeNe laser. A minor uncertainty (10%) origins presumably from the fact that only slightly more than one interference fringe could be

traced by the maximum deflection of the micromirrors. For future optimizations, a more precise calibration should be possible by multiple reflections to gain further modulation cycles or by white light interferometry. The latter should also yield an exact representation of the complete MEMS surface, and therefore a general offset frame to actively flatten the structure above its passive planarity.

C. Autocorrelator

The main design target of the applied characterization device was the ability for fast inspection and tuning of key components such as the compressor or the shaper assembly. As these procedures require optical path length variations, a reference free characterization technique is the method of choice. Therefore to facilitate easy adjustments of the setup, a UV autocorrelator assembly has been developed. Its construction relies on TPA in a solar blind photomultiplier cathode made for VUV radiation detection. To further simplify the autocorrelator, the device is based on a split mirror design, which has already proven versatile for ultrashort pulse characterization in the literature over the last years [18,26–29]. In this setup the beam splitting is realized by spatial cutting the beam profile in two halves by a split mirror. To collect autocorrelation traces, one half mirror is moved by a piezostage. The stage is operated in an open loop configuration, and the position is measured by a calibrated internal position meter. In this configuration autocorrelation traces can be acquired as fast as four times per second, limited by the available laser repetition rate of 1 kHz. The split beam is focused on the cathode of a solar blind photomultiplier (*Electron Tubes 9423 B*) by an off-axis aluminum mirror (f=101.6 mm). The output of the PMT is amplified and detected by Boxcar integration. The presented autocorrelator shows an excellent everyday usability owing to the reduced quantity of degrees of freedom to adjust. This concept is further assisted by the application of a TPA nonlinearity, as no phase-matching adjustments are required for this process.

The built-in low-noise amplification of photoelectrons makes a photomultiplier an ideal two-photon detector for low-energy pulse characterization. In case of our setup, energies below 15 pJ in front of the PMT enable the acquisition of an autocorrelation trace. The verification of two-photon behavior of the PMT is shown in Fig. 2(a) at a center wavelength of about 324 nm. A good TPA response with a slope of 1.93 in the double logarithmic plot of PMT against a linear reference diode is observed in the range of typical measurements. A general limit for all two-photon-sensitive detectors is the emerging linear sensitivity toward lower wavelengths. This linear signal contribution of the PMT obscures its TPA response already at wavelengths shifted far from the PMT linear absorption edge. In contrast to nonlinear crystal based autocorrelators, no spectral filtering is possible to discriminate between the fundamental and the two-photon responses of the detector. It is therefore important that the PMT has to be as insensitive as possible to the fundamental wavelength. In case of our setup, AC measurements below 300 nm show significant parasitic linear signal contribution.

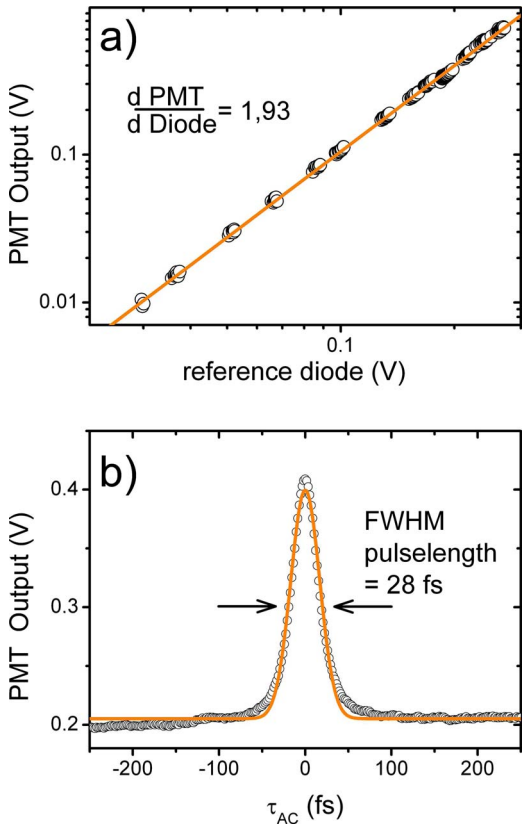

Fig. 2. (Color online) Energy dependence of the PMT response. (a) Linear fit on double logarithmic plot of the data shown in (a) returns a gradient of 1.93 indicating good two photon response of the PMT. (b) A typical AC traces in an energy range covered by (a).

This is noteworthy, as the red edge of the CsI photocathode absorption is around 230 nm [30].

Prior approaches in the literature used high energies (3–20 μJ), partially beyond the damage threshold of the PMT, to acquire an autocorrelation trace [24]. A possible explanation of these high-energy requirements compared with our setup (minimum energy: 15 pJ) may be the quantum efficiency curve of the applied PMT. Its datasheet names only a quantum yield ratio of slightly above 700 between the fundamental and the second harmonic wavelengths for the CsTe photocathode.

In the design of a two-photon photoemission based autocorrelator, the possible contribution of resonance enhanced TPA with finite temporal response should always be considered [31]. As the obtained time bandwidth products agree with the cross correlation data of a similar pulse generation setup [25], the acquired autocorrelations should contain negligible pulse broadening effects owing to noninstantaneous detector response. Nevertheless, in applications for sub-15-fs pulses or for different detectors, the measurement technique should always be reviewed for pulse broadening effects.

An exemplary autocorrelation trace acquired with the split mirror UV autocorrelator discussed in this section is shown in Fig. 2(b). The background contribution resulting from TPA of the two individual pulses is subtracted in subsequent AC figures. A minor baseline drift, as can be seen in Fig. 2(b), can presumably be attributed to weak

shading effects from the moving AC mirror and is also subtracted consecutively. Although the AC setup is capable for real-time monitoring of a tuning process, the measurements shown here are averaged around 1500 laser shots per data point to increase the signal-to-noise ratio. All AC measurements presented were taken in the spectral region between 315 and 330 nm.

3. PHASE-MODULATED UV PULSES

A typical phase-modulator application is the compression of ultrashort pulses. Here we demonstrate the recompression of a femtosecond pulse sent through different amounts of FS glass substrate. Figure 3 shows a scan of the second-order spectral phase tailor term. A 10 or 20 mm FS block is inserted in the beam path of the UV pulse, respectively. By scanning the second-order spectral phase, the pulses are recompressed nearly to the value observed for the unmodified pulse also shown in the figure. The data points shown in Fig. 3 are the measured values, whereas the curve representation is based on fitting a modeled autocorrelation to the data. The fitting relies on the measured spectrum and illustrates that the generated pulses are near the spectral transform limit (TL).

The compensation of a chirp imprinted on a pulse, e.g., by glass substrate, can also be achieved by the application of an adaptive compression scheme based on an evolutionary learning algorithm [32]. This compression experiment serves as a testbed application for closed-loop coherent control runs and illustrates the capability of the presented phase modulator to handle the complex phase functions generated during an evolutionary algorithm run. Figure 4 shows the autocorrelation trace of the UV pulse after an adaptive compression run to compensate 10 mm of FS substrate. The resulting pulse (pulse duration =31 fs) is in excellent agreement compared with the initial pulse (pulse duration=33 fs). To enable fast acquisition, the feedback value for the algorithm is computed from the maximum autocorrelation signal and its baseline. Only these two points of the AC trace are measured to generate the feedback of the adaptive compression.

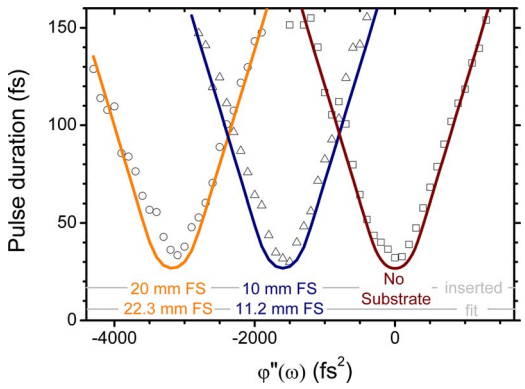

Fig. 3. (Color online) Compensation of dispersion, caused by glass substrates, by second order spectral phase scanning. The curves indicate a fitting based on simulation of an appropriate AC and the retrieved amount of FS is given in comparison to the inserted one.

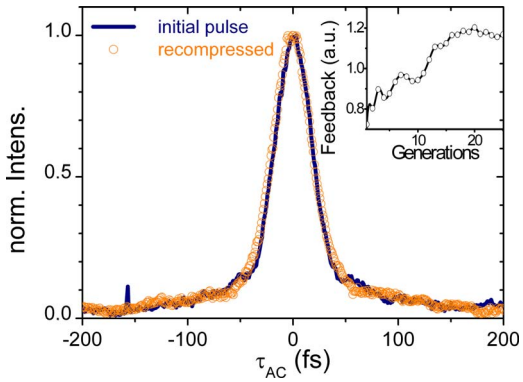

Fig. 4. (Color online) Adaptive recompression after insertion of 10 mm FS substrate into the UV beam path. The figure shows the autocorrelation traces of the optimal pulses with and without the additional substrate. The inset shows the convergence curve of the applied evolutionary algorithm.

The last example demonstrates the generation of multipulses by the application of a sinus modulation of the spectral phase. As multipulses enable the vibrational mode filtering and the control of wave packet motion, they represent an important application for phase modulation technology [33,34]. Figure 5 contains the autocorrelation data of three different multipulse separation values. A pulse is generated from the measured fundamental UV spectrum under the assumption of a flat spectral phase. The comparison between the given and the retrieved values of the multipulse separation shows again a very good agreement. On the average the analysis of the phase

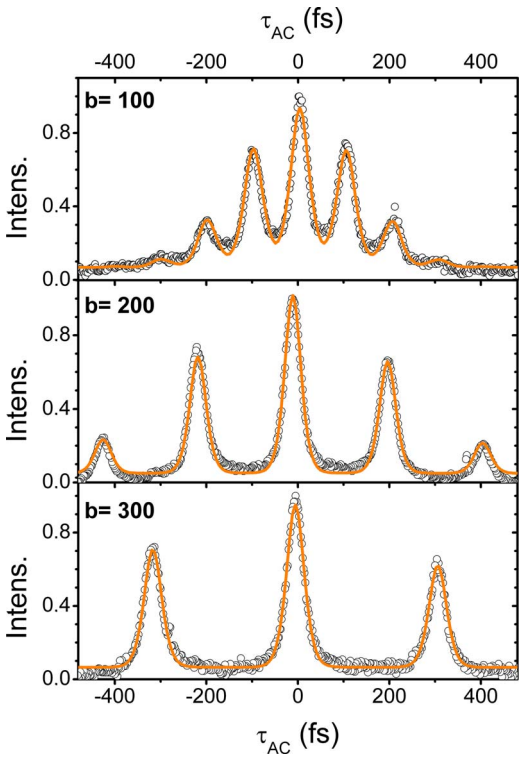

Fig. 5. (Color online) Multipulses generated by sinus phase modulation. The parameters used for multipulse generation correspond to $\phi(\omega)=a\ \sin(\omega b+c)$. (All: $a=1.23$, $c=0$). The points represent the measured AC whereas the curves indicate a fitting based on a simulated AC of the measured pulse spectrum.

modulations in Figs. 4 and 5 exhibits a too low modulation in the range of 5%–10%, indicating a minor calibration error of the phase stroke.

The preceding paragraphs showed the generation of typical phase modulations required in the application of SLM. Furthermore the characterization of the generated UV pulses was realized by the presented AC setup and illustrates the good quality of the obtained measurements. However, in case of shaped pulse forms, the impact of the spatiotemporal characteristics of these beams on split mirror autocorrelation devices has to be carefully analyzed.

In the last part, a more in-depth examination of the interplay between a split mirror autocorrelator and a SLM is given. A typical artifact of pulse phase control is the dependence of spatial effects on temporal modulations [35–39]. As every 4-*f* based phase modulator shows this "space–time coupling," the effects on the applied autocorrelation setup should be carefully analyzed. According to [35] the amount of space–time coupling C_{ST}, described in spatial walk-off per time delay, is given by

$$C_{ST} = \frac{cd\ \cos(\theta_i)}{\lambda},$$

where c is the speed of light, d is the groove spacing of the shaper grating, θ_i is the input angle on this grating, and λ is the center wavelength of the pulse. The formula states that space–time coupling is more pronounced on low dispersive grating setups. Calculation of the space–time coupling on the presented MEMS gives values between 1.5 and 0.7 mm ps^{-1} for 600 and 1200 g mm^{-1} gratings, respectively, for a central wavelength of 330 nm at the Littrow condition (Littrow angles: 11.4° for 1200 g mm^{-1}, 5.7° for 600 g mm^{-1}). With respect to a beam diameter of around 2–3 mm, especially in the case of multipulse generation, the space–time coupling has to be carefully put into consideration.

As previously described, the UV autocorrelator applies spatial beam splitting by a divided mirror. In our standard setup, the split mirror cuts the beam profile perpendicular to the horizontal layer, in which space–time coupling, generated by the phase modulator, takes place. As the phase pattern on the modulator influences the spatiotemporal intensity profile of the beam, each mirror half reflects a different temporal cross section of the beam. In case of a linear phase, generating a simple temporal shift of the pulse, a contrast reduction in the AC trace can be observed. This is correlated with the linear spatial shift of the beam caused by the space–time coupling. This influences the intensity distribution of the two AC beams, resulting in a reduced peak intensity of the AC trace. A more subtle effect can be observed in case of multipulse generation. The initial multipulse measurements appear asymmetric [Fig. 6(a)]. The space–time coupling induces a spatial shift of each temporal subpulse according to its delay [see the illustration in Fig. 6(a)]. Considering the split mirror AC setup used here, a spatial displacement of the subpulses results in an amplitude filtering based on their overlap with the mirror surface. As illustrated in Fig. 6(c), the space–time coupling is hereby roughly approximated by a Gaussian shaped temporal intensity filter simulating

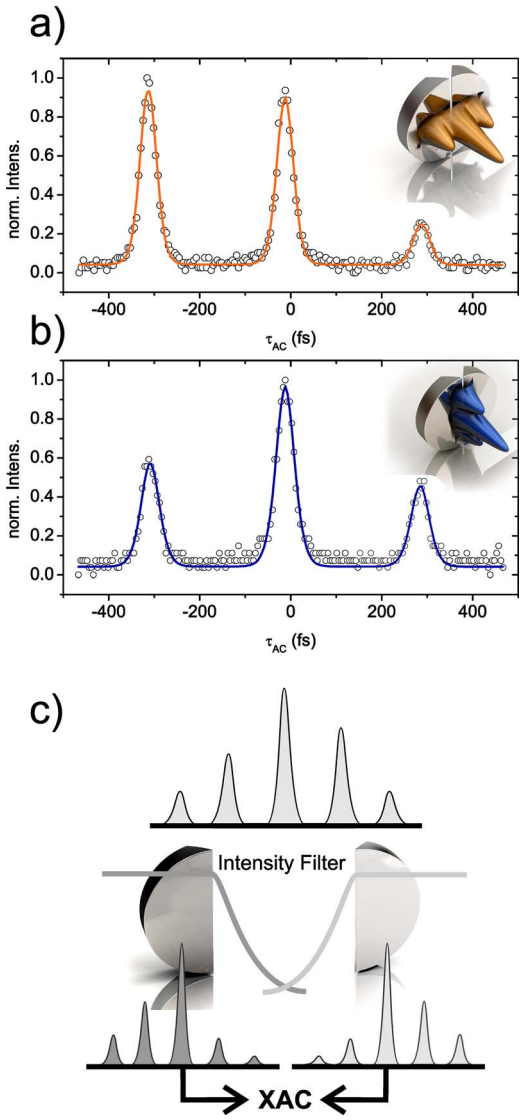

Fig. 6. (Color online) Space–time coupling effect on split mirror autocorrelators: (a) asymmetric autocorrelation trace of multipulse; (b) asymmetry vanishes when beam is rotated by periscope. This effect can be attributed to space–time coupling as illustrated in the insets. The fitting to the asymmetric AC trace is computed according to the illustration in (c). The split mirror acts as intensity filter for the pulse train, yielding an intensity filtered multipulse for each mirror half. A simulated cross correlation between these agrees well with the AC shown in (a).

the edge of each D-shaped mirror. This filter reduces the intensity of subpulses displaced into the gap between the two mirrors. The AC process can therefore be simulated by a cross correlation of the accordingly intensity-modulated pulse trains. Figure 6(a) shows the fitting of measured data by the above-described model. A good agreement between simulation and data is found. The influence of the space–time coupling can be easily checked in the current setup: as the two-photon photoemission and all other optics in the setup are independent on polarization, a periscope can be used to rotate the beam profile by 90° in front of the AC input. In this case the plane of space–time coupling effects does not influence the intensity distribution between the mirror halves. Figure 6(b) illustrates that there is nearly no asymmetry left in

the AC trace, illustrating the vanishing of space–time coupling effects.

4. CONCLUSION

In the present paper we demonstrated a complete setup for the generation of phase-modulated ultrashort pulses and their easy characterization. Starting from a noncollinear parametric amplifier, followed by a sum frequency mixing, a tunable and manageable ultrashort pulse source has been implemented to supply the pulse shaping setup with very short (<30 fs) UV pulses. To generate phase-modulated UV pulses, a MEMS based SLM capable of direct UV phase modulation is applied in reflective 4-*f* geometry. The SLM offers the advantage of a pixelated modulator combined with the potential reflectivity range of a deformable mirror. We illustrated the shaping capability of this device by various phase examples typically found in coherent control applications. Especially, the successful adaptive compression emphasizes the ability of this shaper to generate even complex phase functions.

To test the performance of the constructed system on an everyday basis, an easy applicable autocorrelator for UV pulse characterization has been presented. This device offers a significant improvement in the usability for ultrashort UV pulses in spectroscopic experiments. Particularly the avoidance of external reference pulses makes the technique a valuable tool for ultrashort temporal pulse characterizations at every desired position in an ultrafast UV setup. Additionally, the analysis of split mirror AC trace's symmetry yields an interesting indicator for space–time coupling effects.

ACKNOWLEDGMENTS

The authors thank Steffen Kahra (Max-Planck-Institut für Quantenoptik, Garching, Germany) for valuable discussions at the beginning of this project, which was inspired by his previous work on the MEMS setup. A Ph.D. scholarship of the Philipps-Universität Marburg to J. Möhring is gratefully appreciated. C. S. Lehmann acknowledges a travel grant from the European Science Foundation (ESF-DYNA grant 1796).

REFERENCES

1. H. Rabitz, R. deVivie-Riedle, M. Motzkus, and K.-L. Kompa, "Whither the future of controlling quantum phenomena?" Science **288**, 824–828 (2000).
2. P. Nuernberger, G. Vogt, T. Brixner, and G. Gerber, "Femtosecond quantum control of molecular dynamics in the condensed phase," Phys. Chem. Chem. Phys. **9**, 2470–2497 (2007).
3. M. Hacker, R. Netz, M. Roth, G. Stobrawa, T. Feurer, and R. Sauerbrey, "Frequency doubling of phase-modulated ultrashort laser pulses," Appl. Phys. B **73**, 273–277 (2001).
4. M. Hacker, T. Feurer, R. Sauerbrey, T. Lucza, and G. Szabo, "Programmable femtosecond laser pulses in the ultraviolet," J. Opt. Soc. Am. B **18**, 866–871 (2001).
5. S. Shimizu, Y. Nabekawa, M. Obara, and K. Midorikawa, "Spectral phase transfer for indirect phase control of sub-20-fs deep UV pulses," Opt. Express **13**, 6345–6353 (2005).
6. C. Schriever, S. Lochbrunner, M. Optiz, and E. Riedle, "19 fs shaped ultraviolet pulses," Opt. Lett. **31**, 543–545 (2006).
7. R. Selle, P. Nuernberger, F. Langhojer, F. Dimler, S. Fechner, G. Gerber, and T. Brixner, "Generation of polarization-shaped ultraviolet femtosecond pulses," Opt. Lett. **33**, 803–805 (2008).
8. M. Hacker, G. Stobrawa, R. Sauerbrey, T. Buckup, M. Motzkus, M. Wildenhain, and A. Gehner, "Micromirror SLM for femtosecond pulse shaping in the ultraviolet," Appl. Phys. B **76**, 711–714 (2003).
9. P. Baum, S. Lochbrunner, and E. Riedle, "Tunable sub-10-fs ultraviolet pulses generated by achromatic frequency doubling," Opt. Lett. **29**, 1686–1688 (2004).
10. M. Roth, M. Mehendale, A. Bartelt, and H. Rabitz, "Acousto-optical shaping of ultraviolet femtosecond pulses," Appl. Phys. B **80**, 441–444 (2005).
11. S. Coudreau, D. Kaplan, and P. Tournois, "Ultraviolet acoust-optic programmable dispersive filter laser pulse shaping in KDP," Opt. Lett. **31**, 1899–1901 (2006).
12. B. J. Pearson and T. C. Weihnacht, "Shaped ultrafast laser pulses in the deep ultraviolet," Opt. Express **15**, 4385–4388 (2007).
13. P. Baum, S. Lochbrunner, and E. Riedle, "Zero-additional-phase SPIDER: full characterization of visible and sub-20-fs ultraviolet pulses," Opt. Lett. **29**, 210–212 (2004).
14. P. Nuernberger, G. Vogt, R. Selle, S. Fechner, T. Brixner, and G. Gerber, "Generation of shaped ultraviolet pulses at the third harmonic of titanium-sapphire femtosecond laser radiation," Appl. Phys. B **88**, 519–526 (2007).
15. D. Kane, A. Taylor, R. Trebino, and K. DeLong, "Single-shot measurement of the intensity and phase of a femtosecond UV laser pulse with frequency-resolved optical gating," Opt. Lett. **19**, 1061–1061 (1994).
16. K. Michelmann, T. Feurer, R. Fernsler, and R. Sauerbrey, "Frequency resolved optical gating in the UV using the electronic Kerr effect," Appl. Phys. B **63**, 485–489 (1996).
17. R. Trebino, K. DeLong, D. Fittinghoff, J. Sweetser, M. Krumbügel, B. Richman, and D. Kane, "Measuring ultrashort laser pulses in the time-frequency domain using frequency-resolved optical gating," Rev. Sci. Instrum. **68**, 3277–3295 (1997).
18. C. Durfee III, S. Backus, H. Kapteyn, and M. Murnane, "Intense 8-fs pulse generation in the deep ultraviolet," Opt. Lett. **24**, 697–699 (1999).
19. Y. Takagi, T. Kobayashi, K. Yoshihara, and S. Imamura, "Multiple- and single-shot autocorrelator based on two-photon conductivity in semiconductors," Opt. Lett. **17**, 658–660 (1992).
20. J. Ranka, A. Gaeta, A. Baltuska, M. Pshenichnikov, and D. Wiersma, "Autocorrelation measurement of 6-fs pulses based on the two-photon-induced photocurrent in a GaAsP photodiode," Opt. Lett. **22**, 1344–1346 (1997).
21. A. Streltsov, K. Moll, A. Gaeta, P. Kung, D. Walker, and M. Razeghi, "Pulse autocorrelation measurements based on two- and three-photon conductivity in a GaN photodiode," Appl. Phys. Lett. **75**, 3778–3780 (1999).
22. J. I. Dadap, G. B. Focht, D. H. Reitze, and M. C. Downer, "Two photon absorption in diamond and its application to ultraviolet femtosecond pulse-width measurements," Opt. Lett. **16**, 499–501 (1991).
23. A. M. Streltsov, J. K. Ranka, and A. L. Gaeta, "Femtosecond ultraviolet autocorrelation measurements based on two-photon conductivity in fused silica," Opt. Lett. **23**, 798–800 (1998).
24. K. Ihara, S. Zaitsu, and T. Imasaka, "Autocorrelator consisting of a solar-blind photomultiplier for use in the near-ultraviolet region," Rev. Sci. Instrum. **76**, 026109 (2005).
25. I. Z. Kozma, P. Baum, S. Lochbrunner, and E. Riedle, "Widely tunable sub-30 fs ultraviolet pulses by chirped sum frequency mixing," Opt. Express **11**, 3110–3115 (2003).
26. H. Mashiko, A. Suda, and K. Midorikawa, "All-reflective interferometric autocorrelator for the measurement of ultra-short optical pulses," Appl. Phys. B **76**, 525–530 (2003).
27. I. Z. Kozma, P. Baum, U. Schmidhammer, S. Lochbrunner, and E. Riedle, "Compact autocorrelator for the online

measurement of tunable 10 femtosecond pulses," Rev. Sci. Instrum. **75**, 2323–2327 (2004).
28. E. Power, J. Pentland, J. Nees, C. P. Hauri, M. Merano, R. Lopez-Martens, and G. Mourou, "All-reflective high fringe contrast autocorrelator for measurement of ultrabroadband optical pulses," Opt. Lett. **31**, 3514–3516 (2006).
29. H. Mashiko, A. Suda, and K. Midorikawa, "Second-order autocorrelation functions for all-reflective interferometric autocorrelator," Appl. Phys. B **87**, 221–226 (2007).
30. "52 mm (2 ") photomultiplier 9423B series data sheet," Electron Tubes, Bury Street Ruislip, Middx, UK.
31. T. Hattori, M. Kawashima, M. Daikoku, H. Inouye, and H. Nakatsuka, "Femtosecond two-photon response dynamics of photomultiplier tubes," Jpn. J. Appl. Phys., Part 2 **39**, 4793–4798 (2000).
32. D. Zeidler, S. Frey, K.-L. Kompa, and M. Motzkus, "Evolutionary algorithms and their application to optimal control studies," Phys. Rev. A **64**, 023420 (2001).
33. A. M. Weiner, D. E. Leaird, G. P. Wiederrecht, and K. A. Nelson, "Femtosecond pulse sequences used for optical manipulation of molecular motion," Science **247**, 1317–1319 (1990).
34. J. Hauer, T. Buckup, and M. Motzkus, "Enhancement of molecular modes by electronically resonant multipulse excitation: further progress towards mode selective chemistry," J. Chem. Phys. **125**, 061101 (2006).
35. M. M. Wefers and K. A. Nelson, "Space-time profiles of shaped ultrafast optical waveforms," IEEE J. Quantum Electron. **32**, 161–172 (1996).
36. T. Tanabe, H. Tanabe, Y. Teramura, and F. Kannari, "Spatiotemporal measurements based on spatial spectral interferometry for ultrashort optical pulses shaped by a Fourier pulse shaper," J. Opt. Soc. Am. B **19**, 2795–2802 (2002).
37. T. Tanabe, F. Kannari, F. Korte, J. Koch, and B. Chichkov, "Influence of spatiotemporal coupling induced by an ultrashort laser pulse shaper on a focused beam profile," Appl. Opt. **44**, 1092–1098 (2005).
38. B. Sussman, R. Lausten, and A. Stolow, "Focusing of light following a 4-f pulse shaper: considerations for quantum control," Phys. Rev. A **77**, 043416 (2008).
39. F. Frei, A. Galler, and T. Feurer, "Space-time coupling in femtosecond pulse shaping and its effects on coherent control," J. Chem. Phys. **130**, 034302 (2009).